Optics Letters

Extension of water-window harmonic cutoff by laser defocusing-assisted phase matching

Cheng Jin,[1,2,7] Ming-Chang Chen,[3,4,6] Hung-Wei Sun,[3] and C. D. Lin[4,5]

[1]Department of Applied Physics, Nanjing University of Science and Technology, Nanjing 210094, China
[2]State Key Laboratory of Transient Optics and Photonics, Xi'an Institute of Optics and Precision Mechanics, Chinese Academy of Sciences, Xi'an 710119, China
[3]Institute of Photonics Technologies, National Tsing Hua University, Hsinchu 30013, Taiwan
[4]Department of Physics, National Tsing Hua University, Hsinchu 30013, Taiwan
[5]J. R. Macdonald Laboratory, Department of Physics, Kansas State University, Manhattan, Kansas 66506, USA
[6]e-mail: mingchang@mx.nthu.edu.tw
[7]e-mail: cjin@njust.edu.cn

Received 17 May 2018; revised 14 August 2018; accepted 16 August 2018; posted 17 August 2018 (Doc. ID 332047); published 11 September 2018

We extend a recently demonstrated scheme [Optica 4, 976 (2017)] to overcome the limit of conventional harmonic cutoff for different pulse durations, laser wavelengths, and gas targets. By tuning the truncation of long wavelength lasers, we show that the defocusing-assisted phase matching (DAPM) can be achieved in a tightly focused beam and highly ionized short gas cell, and can be used to effectively extend the harmonic cutoff energy and optimize its yield. An analysis of phase matching reveals that at longer wavelengths, greater cutoff extension to the water window region is achieved because of the larger harmonic intrinsic phase (proportional to the cube of laser wavelength), and because DAPM works at relatively higher laser intensities using a Ne target. This scheme provides a promising method for efficiently generating intense attosecond light sources in the extreme ultraviolet to x-rays.

OCIS codes: (190.4160) Multiharmonic generation; (190.2620) Harmonic generation and mixing; (190.7110) Ultrafast nonlinear optics; (340.7480) X-rays, soft x-rays, extreme ultraviolet (EUV); (320.7120) Ultrafast phenomena.

https://doi.org/10.1364/OL.43.004433

High-harmonic generation (HHG) in gases offers a coherent tabletop light source spanning from the extreme ultraviolet (XUV) to x-rays with femtosecond or attosecond durations [1]. Except for a few experiments employing soft x-ray HHG [2–4], relatively low-energy XUV photons are still intense enough for most applications. To extend the HHG spectrum to higher photon energies, one feasibility is to use long wavelength lasers, because the cutoff energy of a single-atom HHG spectrum is proportional to λ_L^2, where λ_L is the laser wavelength [5]. However, the harmonic yield from each atom drops significantly, e.g., $\lambda_L^{-(4-6)}$ [6], and further reduction takes place if the propagation of harmonics in the gas medium is taken into account [7]. Although this unfavorable scaling law could be partially compensated by increasing the gas pressure in a gas cell [8–10], shorter-wavelength lasers are still preferable for generating stronger high-order harmonics [11].

Extending the cutoff of HHG can also be carried out with more intense lasers, but excessive ionization will cause phase mismatch between the harmonics and the driving laser, as they propagate in the nonlinear medium to prevent efficient buildup of the macroscopic harmonic field. In a weakly ionized gas medium, the phase mismatch caused by the excessive free electrons can only be compensated by neutral atom dispersion if the ionization level is below the "critical" one [9,10]. This mechanism determines the conventional phase-matching cutoff (CPMC) energy which scales as $\lambda_L^{1.6-1.7}$. Several methods have been proposed to overcome this phase-matching limit, including quasi-phase matching [12,13], neutral atom phase matching [14], and the use of multiple gas jets [15]. Recently, we have demonstrated an alternative to extending the cutoff in Ar by taking advantage of laser defocusing in a gas medium [16]. The self-defocusing of the driving laser [17] and the resulting phase-matching condition at high intensity can be precisely adjusted by truncating an incident Ti-sapphire laser beam. However, such defocusing-assisted phase-matching (DAPM) mechanism has not been verified for other circumstances.

In this Letter, we show that harmonic cutoff can be efficiently extended by truncating input laser beams under different pulse durations in Ar gas or at different laser wavelengths in Ar and Ne gas. We also analyze how the DAPM is achieved in a highly ionized short gas cell due to the existence of laser defocusing.

We first show the simulated macroscopic HHG spectra of Ar in Fig. 1. In the simulation, an initial Gaussian beam with peak intensity of 2.0×10^{10} W/cm^2 and a waist of $w_0 =$ 8 mm is truncated by using an iris before it is focused into a gas cell by a lens with the focal length of 30 cm. A 0.8 mm long uniformly distributed gas cell with the pressure of 50 Torr is placed at the laser focus. The macroscopic propagation of the fundamental laser and the harmonic fields are obtained by solving the three-dimensional Maxwell's equations [7], with the single-atom response calculated from the quantitative rescattering model [18]. We first examine the

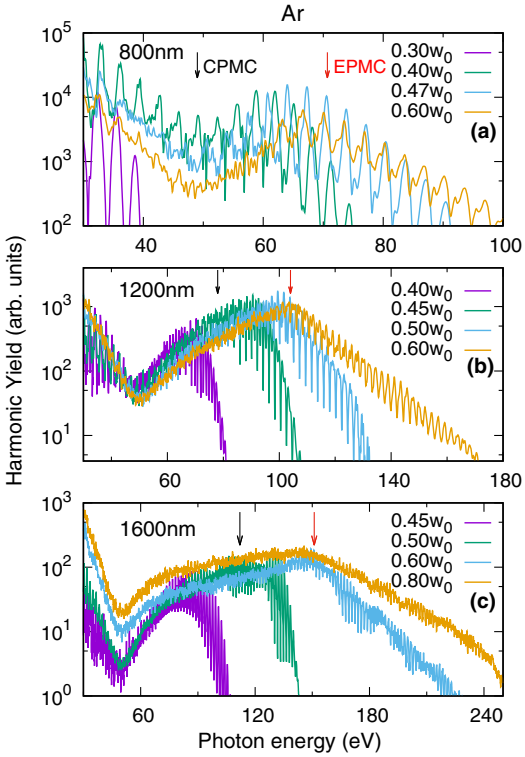

Fig. 1. Harmonic spectra generated in Ar gas by truncated laser beams. The waist of the initial Gaussian beam before being focused is w_0. It is used to label the aperture size of an iris. The black and red arrows indicate the positions of the CPMC and EPMC, respectively. The observed EPMC is where the plateau ends abruptly. See the text for other laser parameters.

HHG spectra by a five-cycle (i.e., 13.3 fs), 800 nm laser pulse. In Fig. 1(a), a clear extended phase-matching cutoff (EPMC) of 70 eV (red arrow) is observed when the iris is set at 0.47 w_0. Compared to the CPMC (black arrow), the cutoff energy is extended by 21 eV. This value is very similar to the extension observed using a longer 25 fs pulse in Ref. [16]. Further increase of the iris opening, i.e., the increase of peak intensity or the decrease of the beam waist at the focus, can no longer extend the cutoff energy. Next, we check the HHG spectra using longer 1200 and 1600 nm wavelengths. The pulse durations are chosen to be five cycles, while other laser parameters are fixed. In Figs. 1(b) and 1(c), the harmonic cutoff energy is progressively increased with a proper aperture size. The EPMC can be identified at 105 and 155 eV for 1200 and 1600 nm lasers, respectively. Comparisons between the CPMC and EPMC for these two wavelengths are given in Table 1. Note that (1) the cutoff extensions indeed occur not only for a short-duration 800 nm pulse, but also for longer-wavelength lasers, e.g., 1200 and 1600 nm; (2) the cutoff extension increases with the laser wavelength; and (3) the harmonic yield in Fig. 1 drops quickly with the laser wavelength in accordance with the wavelength scaling law.

We next analyze the phase-matching mechanism for EPMC harmonics at three wavelengths. We show the time-frequency analysis of off-axis harmonic emission at the exit plane for three wavelengths in Figs. 2(a)–2(c), because the off-axis positions are found to have considerable contribution to the harmonic yield. The figures show that cutoff harmonic emissions are concentrated in the leading edge of the laser pulse. In the trailing edge, the accumulated ionization level becomes too high to limit phase matching. We can also examine the electric fields of the driving laser (in a reference frame moving at the speed of light) at three positions: $z = -0.4$, 0, and 0.4 mm, i.e., at the entrance, middle point, and exit plane of the gas cell, respectively, in Figs. 2(d)–2(f). These figures reveal three important features. First, compared to the field at the entrance, the fields at the middle and the exit are reduced and shifted in time due to the dispersion and the defocusing effect caused by the free electrons in the medium. Secondly, the field change is larger in the first half of the gas cell ($z = -0.4$ to 0 mm) than in the second half ($z = 0$ to 0.4 mm), because the excessive laser intensity (see Table 1) at the entrance needs some propagation distances to decay to a suitable value. Thirdly, electric fields in the second half are close to 0.084 a.u. (the intensity of 2.5×10^{14} W/cm^2), the critical field of Ar [19], above which barrier-suppression ionization dominates, indicating high-level ionization (~10%, much bigger than the "critical" ionization). Figures 2(g)–2(i) demonstrate that the cutoff harmonics (red lines) at three optimal truncations grow steadily from $z = 0$ to 0.4 mm, while the growth of plateau harmonics (green lines) along the propagation distance z is limited.

When a laser pulse is reshaped in the medium, the phase mismatch of HHG can be written as [16,20,21]

$$\Delta k \approx [(q-1)\omega_L \Delta t - \alpha_i \Delta I]/\Delta z, \quad (1)$$

where q is the harmonic order, ω_L is the fundamental laser frequency, and $\alpha_i \Delta I$ accounts for the change of intrinsic dipole phase with laser intensity. For cutoff harmonics, the coefficient $\alpha_i \approx 14 \times 10^{-14}$ rad · cm^2/W for an 800 nm laser [22], and Δt and ΔI are the shifts of the peak electric field in time and intensity variation over a propagation distance Δz, respectively. These values are read from Figs. 2(d)–2(f) and listed in Table 2. Since both Δt and ΔI originated from plasma-induced dispersion and defocusing, the balance between them would minimize the phase mismatch ($\Delta k \simeq 0$), to make dramatic harmonic growth in the medium possible. We call it a

Table 1. Critical Ionization Level (η) and Photon Energies of the CPMC and EPMC for Ar and Ne at Different Wavelengths[a]

Gas	λ_L	η	CPMC	EPMC	$\Delta\omega$	A	I
Ar	800 nm	3.6%	49 eV	70 eV	21 eV	0.47w_0	5.5I_0
	1200 nm	1.6%	78 eV	105 eV	27 eV	0.50w_0	3.0I_0
	1600 nm	0.90%	112 eV	155 eV	43 eV	0.60w_0	3.2I_0
Ne	800 nm	0.87%	106 eV	155 eV	49 eV	0.65w_0	16.6I_0
	1600 nm	0.22%	272 eV	355 eV	83 eV	0.80w_0	7.8I_0

[a]$\Delta\omega$ is the value of the cutoff extension. The CPMC is determined by a peak intensity, at which the ionization of a five-cycle pulse reaches the critical level. The optimal aperture size (A) is labeled with respect to the initial beam waist w_0, and the corresponding peak intensity (I) at the focus (in the vacuum) is shown. $I_0 = 10^{14}$ W/cm^2.

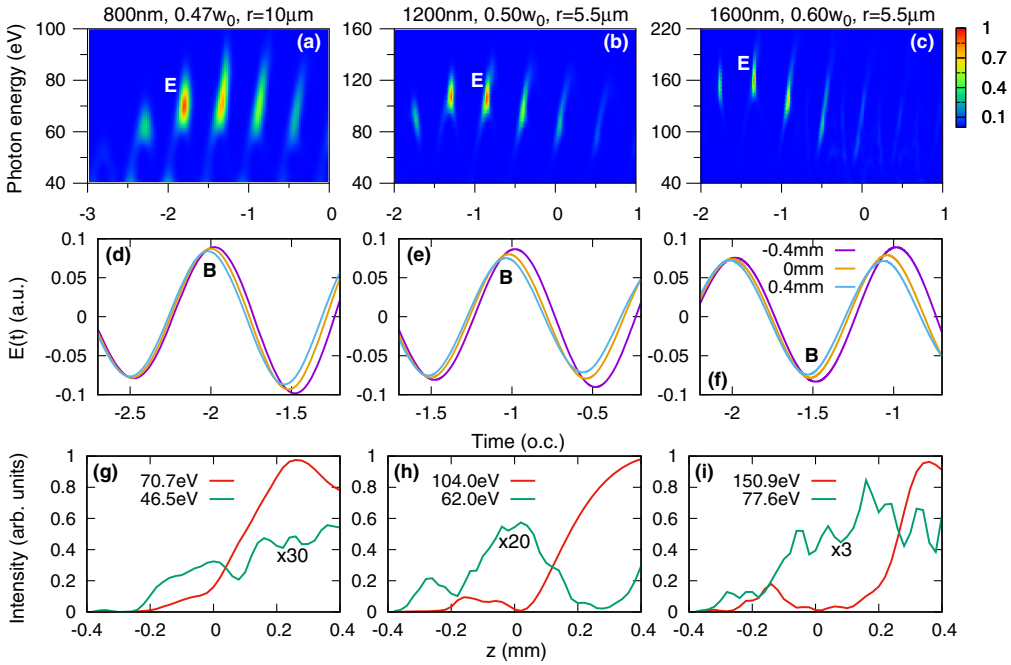

Fig. 2. (a)–(c) Time-frequency analysis of harmonic emission of Ar at off-axis positions of the exit plane, where the EPMC harmonic is most intense when the iris is at optimal truncation (indicated on the top of figures). (d)–(f) Off-axis electric fields shown at the entrance ($z = -0.4$ mm), center ($z = 0$ mm), and exit ($z = 0.4$ mm) planes of the gas cell. (o.c., optical cycle of the laser). (g)–(i) Evolution of the selected cutoff and plateau harmonics with the propagation distance z. The electric fields labeled by "B" are related to the strongest emission labeled by "E."

DAPM mechanism. From $z = -0.4$ to 0 mm, severe laser defocusing results in a much larger ΔI over a propagation distance Δz. Even though the laser intensity can generate the cutoff far beyond the EPMC, the harmonic yield cannot efficiently grow. In the second half of the gas cell, over an identical distance Δz, ΔI becomes smaller, roughly fulfilling $\Delta t/\Delta I \simeq \alpha_i/(q-1)\omega_L$, thus making the DAPM occurring at EPMC. This is further confirmed by the numerical analysis in the following. For the 800 nm case, the coherence length L_{coh} is about 0.5 mm for the 70.7 eV harmonic shown in Table 2, which is consistent with the harmonic growth observed in Fig. 2(g). For the 1200 nm (or 1600 nm) case, compared to 800 nm, ΔI does not change much, and Δt is only about 1.3 (or 1.8) times bigger. Meanwhile, $\alpha_i \propto \lambda_L^3$ [23] is 3.375 (or 8.0) times bigger. Therefore, $(q-1)\omega_L$ in Eq. (1) is increased, leading to a similar coherence length as the 800 nm case. The increase becomes more significant for a longer wavelength. This explains the cutoff energy increases with the laser wavelength in Fig. 1. The coherence lengths are about 0.6 and 0.8 mm for the cutoff harmonics by 1200 and 1600 nm lasers, respectively, which agree with the evolution of the harmonic with z from $z = 0$ to 0.4 mm in Figs. 2(h) and 2(i). The coherence lengths calculated at the three wavelengths also indicate that the DAPM mechanism needs a short gas medium.

We also simulated macroscopic HHG spectra in Ne gas using five-cycle 800 and 1600 nm laser pulses; see Fig. 3. Other laser parameters are fixed. The EPMC occurs for the truncation of 0.65 and 0.80w_0, for the two given wavelengths, leading to tighter and more intense beams (see Table 1) in the interaction region compared to those in Ar. For the 1600 nm laser, it gives

Table 2. Coherence Length of the EPMC Harmonic, Defined by $L_{\text{coh}} = \pi/|\Delta k|$, with Δk Calculated by Eq. (1)[a]

Gas	λ_L	Δt (as)	ΔI (I_0)	EPMC	L_{coh}
Ar	800 nm	−53	−0.205	70.7 eV	0.5 mm
	1200 nm	−68	−0.272	104.0 eV	0.6 mm
	1600 nm	−96	−0.209	159.6 eV	0.8 mm
Ne	800 nm	−107	−1.533	156.7 eV	0.3 mm
	1600 nm	−145	−0.630	351.3 eV	0.2 mm

[a]The temporal shift of the peak electric field (Δt) and the change of the peak intensity (ΔI) from $z = 0$ to 0.4 mm around "B" labeled in Figs. 2(d)–2(f) and 4(c)–4(d). $I_0 = 10^{14}$ W/cm^2.

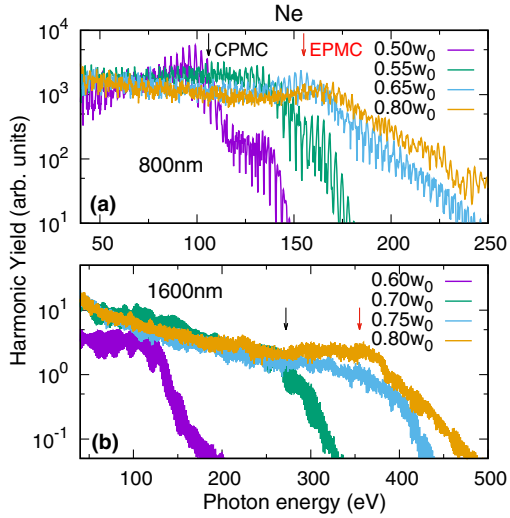

Fig. 3. HHG spectra of Ne obtained by truncated 800 and 1600 nm laser beams. The size of the truncation is indicated by using w_0. The black and red arrows indicate the CPMC and EPMC positions, respectively.

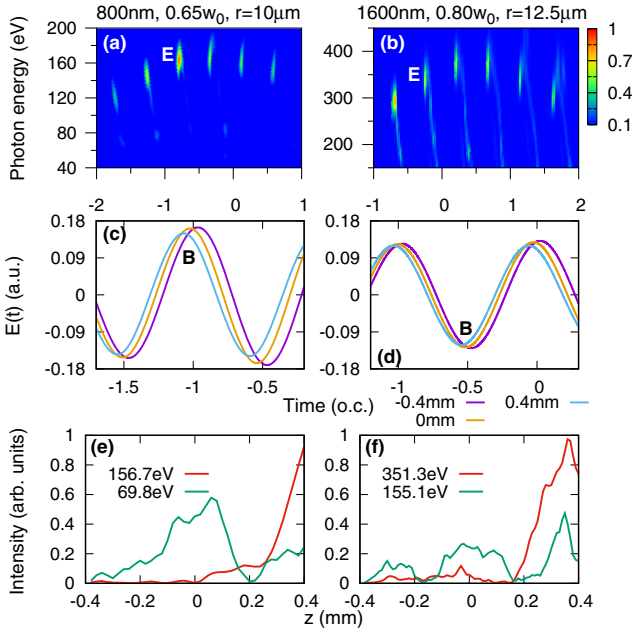

Fig. 4. (a) and (b) Time-frequency analysis of harmonic emission in Ne at off-axis positions of the exit plane. (c) and (d) Off-axis electric fields shown at different positions of the gas cell. (e) and (f) Evolution of the selected cutoff and plateau harmonics with the propagation distance z. (o.c., optical cycle of the driving laser.) The electric fields around "B" are used to compute the coherence length, which are related to the strongest emission labeled by "E."

the EPMC at 355 eV, right in the "water window" region. We have checked that further changing the truncation would neither increase the yield nor the photon energy of the extended cutoff. From the time-frequency analysis of off-axis harmonic emission at the exit plane shown in Figs. 4(a) and 4(b), we pick up the strongest emissions for EPMC harmonics (label "E"), and their ionization time can be traced back to Figs. 4(c) and 4(d) (label "B"). We also note that in these figures the electric fields in the second half are either above or a little bit less than the critical field of 0.16 a.u. for Ne (the corresponding intensity of 8.6×10^{14} W/cm^2) [19], and the corresponding ionization level is ~5%, much bigger than the "critical" value in Table 1. Since Ne has a higher ionization potential, high harmonics are generated at relatively higher laser intensity. As shown in Table 2, ΔI is about three and seven times larger than those in Ar for 800 and 1600 nm lasers, respectively. Meanwhile, Δt is only 1.5 or 2 times larger. This would make the DAPM to occur at a larger $(q-1)\omega_L$ in Eq. (1) to satisfy the equation $\Delta t/\Delta I \simeq \alpha_i/(q-1)\omega_L$. In addition, for a 1600 nm laser in Ne, α_i is eight times larger than the 800 nm laser, thus extending the phase-matched harmonics into the "water window." Table 2 shows the calculated coherence lengths for the selected EPMC harmonics in Ne. The growth of these harmonics by the DAPM is confirmed also in Figs. 4(e) and 4(f).

In summary, we demonstrated the DAPM mechanism in a highly ionized and short gas medium. The optimal phase-matching conditions can be achieved by tuning the aperture size of the iris to truncate the incident laser beam into a tightly focused one. This may not be the only way to realize the DAPM. Therefore, it is motivated to engineer the spatial beam profile that manipulates the plasma-induced defocusing for highly efficient cutoff extension. Very recently, a similar method of reshaping the driving laser pulse in a strongly ionized medium to generate "water-window" harmonics has been demonstrated experimentally [24]. These proposed schemes can overcome the conventional limit set by the "critical" ionization level and greatly extend the harmonic cutoff, to pave the way for generating table–top high-flux high harmonics in a variety of spectral regions.

Funding. Fundamental Research Funds for the Central Universities of China (30916011207); National Natural Science Foundation of China (NSFC) (11774175); Ministry of Science and Technology, Taiwan (MOST) (105-2112-M-007-030-MY3); Chemical Sciences, Geosciences and Biosciences Division, Office of Basic Energy Sciences, Office of Science, U.S. Department of Energy (DOE) (DE-FG02-86ER13491).

REFERENCES

1. F. Krausz and M. Ivanov, Rev. Mod. Phys. **81**, 163 (2009).
2. A. R. Attar, A. Bhattacherjee, C. D. Pemmaraju, K. Schnorr, K. D. Closser, D. Prendergast, and S. R. Leone, Science **356**, 54 (2017).
3. Y. Pertot, C. Schmidt, M. Matthews, A. Chauvet, M. Huppert, V. Svoboda, A. von Conta, A. Tehlar, D. Baykusheva, J.-P. Wolf, and H. J. Wörner, Science **355**, 264 (2017).
4. S. L. Cousin, N. Di Palo, B. Buades, S. M. Teichmann, M. Reduzzi, M. Devetta, A. Kheifets, G. Sansone, and J. Biegert, Phys. Rev. X **7**, 041030 (2017).
5. B. Shan and Z. Chang, Phys. Rev. A **65**, 011804 (2001).
6. J. Tate, T. Auguste, H. G. Muller, P. Salières, P. Agostini, and L. F. DiMauro, Phys. Rev. Lett. **98**, 013901 (2007).
7. C. Jin, A. T. Le, and C. D. Lin, Phys. Rev. A **83**, 023411 (2011).
8. T. Popmintchev, M.-C. Chen, D. Popmintchev, P. Arpin, S. Brown, S. Ališauskas, G. Andriukaitis, T. Balciunas, O. D. Mücke, A. Pugzlys, A. Baltuška, B. Shim, S. E. Schrauth, A. Gaeta, C. Hernández-García, L. Plaja, A. Becker, A. Jaron-Becker, M. M. Murnane, and H. C. Kapteyn, Science **336**, 1287 (2012).
9. T. Popmintchev, M.-C. Chen, A. Bahabad, M. Gerrity, P. Sidorenko, O. Cohen, I. P. Christov, M. M. Murnane, and H. C. Kapteyn, Proc. Natl. Acad. Sci. USA **106**, 10516 (2009).
10. M.-C. Chen, P. Arpin, T. Popmintchev, M. Gerrity, B. Zhang, M. Seaberg, D. Popmintchev, M. M. Murnane, and H. C. Kapteyn, Phys. Rev. Lett. **105**, 173901 (2010).
11. H. Wang, Y. Xu, S. Ulonska, J. S. Robinson, P. Ranitovic, and R. A. Kaindl, Nat. Commun. **6**, 7459 (2015).
12. E. A. Gibson, A. Paul, N. Wagner, D. Gaudiosi, and S. Backus, Science **302**, 95 (2003).
13. X. Zhang, A. L. Lytle, T. Popmintchev, X. Zhou, H. C. Kapteyn, M. M. Murnane, and O. Cohen, Nat. Phys. **3**, 270 (2007).
14. E. J. Takahashi, T. Kanai, K. L. Ishikawa, Y. Nabekawa, and K. Midorikawa, Phys. Rev. Lett. **101**, 253901 (2008).
15. J. Seres, V. S. Yakovlev, E. Seres, C. Streli, P. Wobrauschek, C. Spielmann, and F. Krausz, Nat. Phys. **3**, 878 (2007).
16. H.-W. Sun, P.-C. Huang, Y.-H. Tzeng, R.-T. Huang, C. D. Lin, C. Jin, and M.-C. Chen, Optica **4**, 976 (2017).
17. C. J. Lai and F. X. Kärtner, Opt. Express **19**, 22377 (2011).
18. A. T. Le, R. R. Lucchese, S. Tonzani, T. Morishita, and C. D. Lin, Phys. Rev. A **80**, 013401 (2009).
19. X. M. Tong and C. D. Lin, J. Phys. B **38**, 2593 (2005).
20. M. Geissler, G. Tempea, and T. Brabec, Phys. Rev. A **62**, 033817 (2000).
21. C. Jin and C. D. Lin, Phys. Rev. A **94**, 043804 (2016).
22. M. B. Gaarde and K. J. Schafer, Phys. Rev. A **65**, 031406 (2002).
23. M. Lewenstein, P. Salieres, and A. L'Huillier, Phys. Rev. A **52**, 4747 (1995).
24. A. S. Johnson, D. R. Austin, D. A. Wood, C. Brahms, A. Gregory, K. B. Holzner, S. Jarosch, E. W. Larsen, S. Parker, C. S. Strüber, P. Ye, J. W. G. Tisch, and J. P. Marangos, Sci. Adv. **4**, eaar3761 (2018).